Published in final edited form as:

J Bone Miner Res. 2023 January ; 38(1): 171–185. doi:10.1002/jbmr.4746.

Protein Kinase G2 Is Essential for Skeletal Homeostasis and Adaptation to Mechanical Loading in Male but not Female Mice

Hema Kalyanaraman[1,3], **Shyamsundar Pal China**[1,3], **Justin A. Cabriales**[1], **Jafar Moininazeri**[1], **Darren E. Casteel**[1], **Julian J. Garcia**[1,2], **Van W. Wong**[2], **Albert Chen**[2], **Robert L. Sah**[2], **Gerry R. Boss**[1], **Renate B. Pilz**[1,*]

[1]Department of Medicine, University of California, San Diego, La Jolla, CA 92093, USA

[2]Department of Bioengineering, University of California, San Diego, La Jolla, CA 92093, USA

[3]These two authors contributed equally to the work

Abstract

We previously showed that the NO/cGMP/protein kinase G (PKG) signaling pathway positively regulates osteoblast proliferation, differentiation, and survival *in vitro*, and that cGMP-elevating agents have bone-anabolic effects in mice. Here, we generated mice with an osteoblast-specific (OB) knockout (KO) of type 2 PKG (gene name *Prkg2*) using a Col1a1(2.3kb)-Cre driver. Compared to wild type littermates, eight week-old male OB *Prkg2*-KO mice had fewer osteoblasts, reduced bone formation rates, and lower trabecular and cortical bone volumes. Female OB *Prkg2*-KO littermates showed no bone abnormalities, despite the same degree of PKG2 deficiency in bone. Expression of osteoblast differentiation- and Wnt/β-catenin-related genes was lower in primary osteoblasts and bones of male KO but not female KO mice compared to wild type littermates. Osteoclast parameters were unaffected in both sexes. Since PKG2 is part of a mechano-sensitive complex in osteoblast membranes, we examined its role during mechanical loading. Cyclical compression of the tibia increased cortical thickness and induced mechanosensitive and Wnt/β-catenin-related genes to a similar extent in male and female wild type mice and female OB *Prkg2*-KO mice, but loading had a minimal effect in male KO mice. We conclude that PKG2 drives bone acquisition and adaptation to mechanical loading via the Wnt/β-catenin pathway in male mice. The striking sexual dimorphism of OB *Prkg2*-KO mice suggests that current FDA-approved cGMP-elevating agents may represent novel effective treatment options for male osteoporosis.

Keywords

Genetic animal model; Molecular pathways – remodeling; Osteoblasts; Wnt/β-catenin; Analysis – other (mechanical loading)

*Corresponding Author: Renate B. Pilz, rpilz@ucsd.edu, University of California, San Diego, 9500 Gilman Dr., La Jolla, CA 92093-0652. Phone: 858-534-8805, Fax: 858-534-1421.

AUTHOR CONTRIBUTIONS: Study design: HK and RBP. Study conduct: HK, SPC, JC, JM, DEC, and JJG. Data collection: HK, SPC, JC, VWW, AC, and JM. Data analysis: HK, SPC, GRB, and RBP. Data interpretation: HK, SPC, RLS, GRB, and RBP. Drafting manuscript: HK and RBP. HK, SPC, and RBP take responsibility for the integrity of the data analysis.

COMPETING INTERESTS: The authors declare no conflicts of interest.

INTRODUCTION

Skeletal homeostasis requires continuous remodeling of bone, with the balance between bone formation and resorption controlled by systemic hormones and locally-produced factors. Bone-forming osteoblasts are derived from mesenchymal stem cells; they secrete matrix proteins, e.g., type I collagen and osteocalcin, deposit hydroxyapatite, and differentiate into matrix-embedded, interconnected osteocytes, which are uniquely sensitive to mechanical stimulation.[1,2] Bone-resorbing osteoclasts are derived from hematopoietic precursors; they secrete proteases and hydrogen ions and their differentiation is controlled by osteoblast-derived factors such as receptor activator of nuclear factor-κB ligand (RANKL) and osteoprotegerin (OPG).[1]

Cultured osteoblasts produce nitric oxide (NO) in response to mechanical stimulation, and after exposure to estrogen, insulin, or thyroid hormone,[3–8] while osteoclasts produce NO in response to RANKL.[9] NO can signal via protein nitrosylation and nitration, but a main intracellular target is guanylyl cyclase-1, which produces cGMP.[10] The latter regulates two types of protein kinase G - cytosolic PKG1 and plasma membrane-bound PKG2 - as well as phosphodiesterases and ion channels.[11] *In vitro*, PKG activation in cells of osteoblast lineage enhances proliferation, differentiation, and survival, whereas PKG activation in osteoclasts inhibits their adhesion and acid secretion.[11,12]

NO and cGMP have anabolic effects in bone, but whether they have differential effects in males and females is unclear. NO donors maintain bone mass in estrogen-deficient mice and rats, and nitric oxide synthase (NOS) inhibitors limit estrogen-induced bone formation.[11,13–15] Cinaciguat, a NO-independent guanylyl cyclase-1 activator, prevents bone loss in female ovariectomized and male diabetic mice via a cGMP-induced increase in bone formation and decrease in bone resorption.[8,16,17] Similarly, inhibition of cGMP breakdown by phosphodiesterase-5 inhibitors has bone anabolic effects in intact and ovariectomized mice.[18,19] NOS-3 knockout mice generally have a reduced number of osteoblasts and impaired osteoblast maturation, leading to low bone mass that improves with NO donors, but some *Nos3*$^{-/-}$ strains show accelerated bone loss only after ovariectomy.[20–22] In humans, epidemiological studies suggest that NO-generating nitrates reduce fracture risk.[23–25] Nitrates can increase bone formation markers and bone mineral density in postmenopausal women; however, transdermal nitroglycerin did not affect bone mineral density in a large randomized, placebo-controlled trial.[26–29]

NO/cGMP signaling mediates pro-proliferative and anti-apoptotic responses to fluid shear stress in vitro in osteoblasts and osteocytes, respectively.[5,30–32] We showed that NO/cGMP signaling activates ERK1/2 and Akt in shear-stressed osteoblasts via a membrane complex composed of PKG2, Src, SHP1/2, and integrin β3, and that PKG2 is required for osteoblast proliferation after mechanical stimulation *in vitro*.[5,32] NO also mediates mechanotransduction *in vivo*, because bone formation induced by reloading hindlimbs after tail suspension is defective in NOS-2 knockout mice and suppressed by pharmacological NOS inhibition in wild type animals.[33]

Global knockout of PKG2 (gene name *Prkg2*) impairs chondroblast differentiation and skeletal growth, and PKG2-deficient rodents and humans are dwarfs.[11,34–36] To study the precise role of cGMP/PKG2 in osteoblasts *in vivo*, we generated osteoblast-specific *Prkg2* knockout (OB-*Prkg2*-KO) mice. We found that the males, but not the females, had decreased rates of bone formation and low bone mass, and reduced cortical thickening in response to cyclical tibial loading. Male and female mice with genetic defects in bone-relevant networks can show differences in their basal skeletal phenotype, although the mechanism(s) underlying these differences are not well understood.[37] The striking sexual dimorphism we observed in the OB-*Prkg2*-KO mice could be explained by PKG2 controlling Wnt/β-catenin-related gene expression in males, but not females.

MATERIALS AND METHODS

Materials.

Primary antibodies are described in Suppl. Table 1. Alizarin complexone, 5-bromo-2-deoxyuridine (BrdU), deoxyribonuclease-1, and calcein were from Millipore Sigma, and 8-(4-chlorophenylthio)-cGMP (8-pCPT-cGMP) was from BioLog. A methylmethacrylate embedding kit was from Dorn & Hart Microedge, Inc.

Generation of osteoblast-specific PKG2 knockout mice (OB Prkg2-KO).

We targeted exon 3 of PKG II for deletion (Suppl. Fig. 1a), because: (i) this exon encodes the first part of the cGMP binding pocket, (ii) no alternative splicing occurs here, and (iii) excision results in a frame-shift (*Prkg2*, gene ID 19092). To generate $Prkg2^{f/f}$ mice, we PCR-amplified genomic DNA fragments encoding *Prkg2* exon 3 with flanking sequences from 129/SvJ ES cells using KOD polymerase (EMD Millipore Corporation). The *Prkg2*-floxed construct was assembled in the vector pDLNL (gift from J. Chen of UCSD) and consisted of a 4.2 kb 5’ arm, a 0.55 kb fragment including exon 3 flanked by LoxP sites, a 1.3 kb *neo* cassette flanked by FRT sites, and a 3 kb 3’ arm. All PCR-generated genomic fragments and fusion sites were sequenced. The lineralized construct was electroporated into mouse 129/SvJ (R1) ES cells, which were selected in G418 for homologous recombination of the targeting vector; homologous recombination was confirmed by Southern blot analysis using probes outside of the 5’ and 3’ arms. Blastocyst injection, implantation, and germline transmission was conducted at the UC San Diego Transgenic and Gene Targeting Core. Chimeras were bred to produce pre-mutant $Prkg2^{f\text{-}NEO/+}$ mice, which were bred with mice expressing FLP recombinase (FLPeR mice from Jackson Laboratories) to remove the neomycin cassette. Presence of the conditional “floxed” allele without the neomycin cassette was confirmed by Southern blotting using KpnI-digested DNA from tail biopsies and a probe located in the 3’ homologous arm of the targeting vector (P3’, Suppl. Fig. 1a,b). The $Prkg2^{f/+}$ mice were back-crossed for nine generations into the C57BL/6NHsd background (Envigo #044), and then bred to produce homozygous $Prkg2^{f/f}$ mice. The floxed allele was detected by PCR using the primers 5’-GCATAAGCACATCAATGGAGG-3’ and 5’-AGGAAAGCAGGAAAGATTCAC-3’, which span the 5’LoxP site and generate a 459 bp product (Suppl. Fig. 1c).

Osteoblast-specific *Prkg2*-KO mice were obtained by crossing *Prkg2*$^{f/f}$ mice with transgenic mice expressing CRE recombinase under control of the 2.3-kb collagen type-1α1 promoter [B6.Cg-Tg(col1a1-cre)-Haak mice from RIKEN BioResource Research Center (RBRC05524), also in a C57BL/6 background].[38] The CRE transgene was detected with the following primers: 5'-CAAAACAGGCTCTAGCGTTC-3' and 5'-TCGACCAGTTTAGTTACCCC-3'.

Animal experiments.

All mouse experiments were approved by the Institutional Animal Care and Use Committee of the University of California, San Diego. Mice were housed at 3–4 animals per cage in a temperature-controlled environment with a 12 h light/dark cycle and *ad libitum* access to water and food (Teklad Rodent Diet #8604). Experiments described in Figs. 1–4 were performed in eight week-old male and female mice (Cohort 1, including mice with the genotypes *Prkg2*$^{f/f}$ and *Col1a1-Cre; Prkg2*$^{f/f}$), which were injected intraperitoneally with calcein (25 mg/kg) seven and two days prior to euthanasia. Mice were euthanized between 8 am and noon, using CO_2 asphyxiation and exsanguination.

Strain gauge analyses.

Preliminary strain-load relationship studies were performed on a separate cohort of 20 week-old mice (Cohort 2, n= 3 per group of male and female *Prkg2*$^{f/f}$ mice and male *Col1a1-Cre; Prkg2*$^{f/f}$ mice), using axial tibial compression as described.[39] Skeletally-mature mice were used for loading experiments to exclude possible effects on growth and minimize the risk of injury. The animals were kept anesthetized with 2% isoflurane throughout the procedure and were euthanized after loading. The anteromedial surface of the left tibia was exposed by a small incision, the periosteum was removed, and the bone surface was degreased with chloroform. A strain gauge (MMF327634 L2A-13-015LW-120, Vishay, Micro-Measurements) was attached to the anteromedial tibial mid-shaft aligned with the tibial long axis using cyanoacrylate adhesive (Permabond 101™), and the gauge was coated with the epoxy Araldite Rapid™. The gauge was connected to the computer via a screw terminal adapter (Vishay, MM120-001637 RJ45-STA) and the DAQ Data Acquisition Device (Vishay, MM01-120) configured for a quarter-bridge strain gauge element. The mice were positioned in the loading device described below, such that the loading piston applied a compressive load through contacts at the knee and ankle.[40] The tibia was loaded in 1N increments from 4N to 10N, with strain measurements recorded and analyzed using MM01 Multi DAQ software (Vishay, Micro-Measurements); the maximum strain from each load peak was plotted in a load versus strain curve. We found that 8N load in male and 7N load in female *Prkg2*$^{f/f}$ mice produced approximately 1400 με strain in the anteromedial mid-diaphyseal surface of the tibia (Suppl. Fig. 6a), similar to results reported in 17 week-old male and female C57BL/6 wild type mice.[41]

In vivo tibial loading.

Tibial loading experiments were performed with two groups of 20 week-old mice (Cohorts 3 and 4). Male and female OB *Prkg2*-KO mice and their *Prkg2*-WT litter mates (28–35 g males and 23–27g females) were anesthetized with 2% isofluorane and subjected to cyclic compressive forces applied to the left tibia using an actuator fitted with custom fixtures to

hold the hindlimb with the knee and ankle flexed to ~50–60°;[40] the tibia was maintained in the loading device using a 1 N pre-load (Fig. 6a,b). The loading protocol consisted of 220 compressive triangle waveform loads administered at 4 Hz and characterized by 0.15 sec of symmetric loading/unloading with a 0.1 sec dwell (at 1 N) between each of 4 cycles and a 5 sec rest period between sets of 4 cycles, applied 5 days per week over two weeks (Fig. 6b,c).[42] Mice in Cohort 3 were injected intraperitoneally with calcein (25 mg/kg) and alizarin complexone (50 mg/kg), on days 8 and 12, respectively, after the start of the loading protocol and were euthanized on day 15 (Fig. 6c). Mice in Cohort 4 were subjected to the same loading protocol, but they were euthanized three hours after a single loading episode for RNA extraction (Fig. 6h).

The loading pattern (wave form, number of cycles, and loading duration) was adopted based on results of Young et al.,[42] and is similar to well-established loading protocols.[40] Peak loads of 8 N (for males) and 7 N (for females) were chosen to produce similar strains of ~1400 με in male and female mice, and to induce lamellar rather than woven bone formation. Preliminary studies showed that higher peak loads led to joint injuries and rarely to fibula fractures, and were associated with exuberant woven bone formation. Two *Prkg2*-WT mice (one male and one female) and three OB *Prkg2*-KO mice (two male and one female) were excluded from analysis because of injury, perhaps due to improper operation of the loading device, causing persistent limping after recovery from anesthesia; these mice were euthanized. Ankle swelling has been reported even with relatively low peak strains.[43] Previous studies have established that a 1 N pre-load does not have any osteogenic effects, and that there is no effect of loading on the contralateral control limb.[41,42]

Primary osteoblast (POB) cultures.

POBs were isolated from femurs and tibiae of 12 week-old mice (Cohort 5, 12 week-old mice were used to maximize cell yield). POBs were cultured in Dulbecco's modified Eagle's medium (DMEM) supplemented with 10% fetal bovine serum (FBS) as described.[13] To induce differentiation, cells were plated at high density, and after reaching a confluent state were switched to medium with 0.3 mM sodium ascorbate and 10 mM β-glycerophosphate. Each POB preparation was characterized by alkaline phosphatase staining and mineralization capacity as described;[13] cells were used at passages 1–3.

Quantitative RT-PCR.

Epiphyses at both ends of the tibia were cut off with a scalpel to remove the growth plates, and bone marrow was flushed out of the shafts with 3 ml of ice-cold phosphate-buffered saline using a syringe. The shafts were snap-frozen and pulverized under liquid nitrogen. Bone powder and POBs grown in 6-well dishes were dissolved in Trizol Reagent (Molecular Research Center) for RNA purification, and quantitative RT-PCR was performed with 500 ng (bones) or 1 μg (POBs) of RNA as described.[8] All primers (Suppl. Table 2) were intron-spanning (except 18S rRNA) and tested with serial cDNA dilutions. Genes of interest were normalized to 18S rRNA. The mean ΔCT obtained for male control mice or POBs (genotype $Prkg2^{f/f}$, designated as wild type) was used to calculate relative changes in mRNA using the ΔΔCT method. A separate cohort (Cohort 6) of 12 week-old wild type C57BL/

6NHsd mice (Envigo #044) was used to confirm the observed sex differences in β-catenin target gene expression.

Western blotting, immunofluorescence and immunohistochemical staining.

Western blots were generated using horseradish peroxidase-conjugated secondary antibodies detected by enhanced chemiluminescence.[5] POBs plated on glass coverslips were fixed in 4% paraformaldehyde, permeabilized with 1% Triton-X-100, and incubated with cleaved caspase-3–specific antibody (1:100 dilution), followed by a secondary FITC-conjugated antibody. For BrdU incorporation, cells were incubated with 200 μM BrdU in 0.1% FBS for 24 h; then cells were fixed, permeabilized, and incubated with DNAse I prior to staining with anti-BrdU antibody (1:100 dilution) and secondary Texas Red-conjugated antibody. Nuclei were counterstained with Hoechst 33342, and images were analyzed with a Keyence BZ-X700 fluorescence microscope.

Tibiae were fixed overnight in 10% formalin, decalcified in 0.5 M EDTA (pH 7.5) for 5 d, and embedded in paraffin. Longitudinal sections, 8 μm thick, were de-paraffinized in xylene and rehydrated in graded ethanol and water. For antigen retrieval, slides were placed in 10 mM sodium citrate buffer (pH 6.0) at 80–85°C, and allowed to cool to room temperature for 30 min. Endogenous peroxidase activity was quenched in 3% H_2O_2 for 10 min. After blocking with 5% normal goat serum, slides were incubated overnight at 4°C with anti-PKG2 antibody (1:100), followed by a horseradish peroxidase-conjugated secondary antibody. After development with 3-diaminobenzidine (Vector Laboratories), slides were counterstained with hematoxylin.

Micro-CT.

Ethanol-fixed tibiae were analyzed according to established guidelines,[44] using a Skyscan 1076 (Bruker, Belgium) scanner at 8.78 μm voxel size, and applying an electrical potential of 50 kVp and current of 200 μA, with a 0.5-mm aluminum filter as described.[13] Scanned images were reconstructed to create 3D datasets by NRecon software, and tibiae were uniformly oriented using Dataviewer software. Trabecular bone was assessed by automatic contouring of the proximal tibial metaphysis 0.44 to 1.32 mm distal to the growth plate; an adaptive threshold (0.1788 – 1.668 g/cm^3) was used to select trabecular bone. Cortical bone was analyzed by automatic contouring 4.4 to 5.2 mm distal to the proximal growth plate, using a fixed global threshold (0.542 – 1.668 g/cm^3) to identify cortical bone. Mineral density was determined by calibrating the CTAn histogram setting in reference to images derived from scanning 4 mm diameter hydroxyapatite phantom calibration rods of known mineral density (0.25 g/cm^3 and 0.75 g/cm^3). 3D images were generated from the volume of interest using CTAn and CTVox software.

To compare loaded and unloaded tibiae, cortical bone was analyzed by automatic contouring 2.2 to 4.8 mm (250 to 550 slices) distal to the growth plate, using a global threshold, to capture the portion of the tibia with maximal load-induced cortical bone apposition (Suppl.Fig. 6d).

Histomorphometry.

Osteoblasts and osteoclasts were counted on trabecular surfaces on Masson's Trichrome-stained longitudinal (sagittal) sections of formalin-fixed, decalcified, and paraffin-embedded femurs.[13] Trabecular bone was analyzed between 0.25 and 1.25 mm, and cortical bone between 0.25 and 5 mm proximal to the femoral growth plate; these regions of interest are shown in Suppl. Fig. 3a.[45] For dynamic bone formation analyses of eight week-old mice, double calcein-labelled femurs were fixed in 10% neutral-buffered formalin for 24 h at room temperature and processed in 5% aqueous potassium hydroxide for 96 h at room temperature, to allow longitudinal sectioning of paraffin-embedded, non-decalcified bone samples.[46] The percentage of single- and double-labeled bone surfaces (BS) and the double-calcein interlabel width were measured at trabecular and endocortical surfaces, to calculate mineralizing surface (MS), mineral apposition rate (MAR), and bone formation rate (BFR).[47] Slides were scanned with a Hamamatsu Nanozoomer 2.0 HT Slide Scanning System, and image analysis was performed using the Nanozoomer Digital Pathology NDP.view2 software.

After tibial loading, tibiae were formalin-fixed, dehydrated in ethanol, and embedded in methylmethacrylate; transverse (axial) cross-sections were made with an IsoMet low-speed precision cutter 5 mm below the tibial plateau (4.5 mm distal to the growth plate), and images were taken with a Leica SP8 confocal microscope with lightning deconvolution. Histomorphometric analyses were performed by an observer blinded to the genotype of the mice.

Statistics.

For comparison of two groups, P values refer to unpaired, 2-tailed Student's t test. When the assumption of equal variances was not met, a non-parametric test was done (Mann-Whitney test). For multiple comparisons, P values refer to two-way ANOVA with Holm-Sidak's multiple comparison test as indicated. ANOVA tables with F-values and results of post-hoc tests are provided in Suppl. Table 3. $P<0.05$ was considered statistically significant. Boxplots show 25th and 75th percentiles with whiskers showing minimal and maximal values. Data analysis was performed using GraphPad Prism 8 software.

RESULTS

Osteoblast-specific Prkg2 knockout in mice.

We generated osteoblast-specific *Prkg2* knockout mice by crossing mice carrying floxed *Prkg2* alleles (*Prkg2*$^{f/f}$) with transgenic mice expressing *Cre* recombinase under control of the 2.3 kb collagen type-1α1 (Col1a1) promoter (Suppl. Fig. 1a–c describes the *Prkg2*$^{f/f}$ mice; all mice were in a C57BL/6NHsd background). The Col1a1 promoter is expressed specifically in cells of the osteoblastic lineage, from committed mesenchymal stem cells to mature osteocytes.[48] Osteoblast-specific *Prkg2* knockout mice (OB *Prkg2*-KO: genotype *Col1a1-Cre; Prkg2*$^{f/f}$) had a >85 % reduction in *Prkg2* mRNA and PKG2 protein in tibiae in both males and females compared to age- and sex-matched control litter mates (*Prkg2*-WT: genotype *Prkg2*$^{f/f}$) (Fig 1a and b show mRNA and protein, respectively, for male mice, while data for females are shown in Suppl. Fig. 1d and e; in these and all subsequent figures,

Prkg2-WT and OB *Prkg2*-KO mice are referred to as WT and KO, respectively). *Prkg2* mRNA expression was similar in OB *Prkg2*-KO and *Prkg2*-WT littermates in other organs with high PKG2 expression, i.e., brain, kidney and intestine, and PKG2 protein was readily detected in these tissues (Fig. 1a,c). Immunohistochemical staining of tibial sections showed PKG2 in bone lining cells of *Prkg2*-WT, but not OB *Prkg2*-KO mice (Fig. 1d for males and Suppl. Fig. 1f for females). The amount of type 1 PKG (PKG1) protein in tibiae did not differ between wild type and OB *Prkg2*-KO mice in both sexes (Fig. 1e for males and Suppl. Fig. 1g for females). Experiments reported in Figs. 1–4 were performed on the same cohort of eight week-old mice.

Male OB Prkg2-KO mice have decreased trabecular and cortical bone volumes.

In both males and females, the OB *Prkg2*-KO mice had similar body weights and tibial lengths at eight weeks of age as their *Prkg2*-WT litter mates, with the females weighing ~20% less than the males (Suppl. Fig. 2a,b). Micro-CT analysis of the right tibia showed that male OB *Prkg2*-KO mice had reduced trabecular bone volumes compared to *Prkg2*-WT litter mates, with lower trabecular bone volume fraction, trabecular number and thickness, and bone mineral density (Fig. 2a,b). The male knock-out mice also had reduced cortical bone area fraction and bone area, total cross-sectional area, cortical thickness, and tissue mineral density; however, marrow area did not differ between wild type and knockout mice (Fig. 2c,d). All trabecular and cortical parameters were lower in female *Prkg2*-WT mice compared to their male counterparts, but there were no differences between female *Prkg2*-WT and OB *Prkg2*-KO mice (Fig. 2a–d).

Male OB Prkg2-KO mice have lower osteoblast numbers and bone formation.

Compared to *Prkg2*-WT litter mates, male OB *Prkg2*-KO mice had fewer osteoblasts in trabecular bone and reduced osteoblast activity as reflected by a decreased serum concentration of procollagen-1 N-terminal propeptide (P1NP) (Fig. 3a,b). Females showed no difference in these two parameters between the two genotypes, but had higher osteoblast numbers compared to males (Fig. 3a,b). The number of trabecular osteoclasts was similar in *Prkg2*-WT and OB *Prkg2*-KO mice in both sexes, with slightly more osteoclasts in females (Fig. 3c). The trabecular mineralizing surface (MS/BS), mineral apposition rate (MAR), and bone formation rate (BFR) were reduced in male OB *Prkg2*-KO mice compared to *Prkg2*-WT litter mates as measured by double calcein labeling, with no differences between female *Prkg2*-WT and OB *Prkg2*-KO mice (Fig. 3d, and Suppl. Fig. 3b; Suppl. Fig. 3a shows the regions of interest analyzed for trabecular and cortical bone). Similarly, endocortical MAR and BFR were reduced in male, but not in female OB *Prkg2*-KO mice (Fig. 3e,f).

Cell cycle-, osteoblast differentiation-, and Wnt pathway-related gene transcripts and β-catenin protein are reduced in tibial bone of male OB Prkg2-KO mice compared to Prkg2-WT litter mates.

To investigate potential mechanism(s) underlying the lower bone formation rates and bone volumes in male OB *Prkg2*-KO mice, we examined the expression of genes regulating osteoblast and osteoclast differentiation and function.

Consistent with the reduced number of osteoblasts and reduced osteoblast activity in male OB *Prkg2*-KO mice, we found reduced expression of several sets of genes in tibial shafts of male OB *Prkg2*-KO mice compared to *Prkg2*-WT litter mates: cell cycle-related genes [*Ccnd1* (cyclin D) and *Jun*]; osteoblast differentiation-related genes [*Bglap* (osteocalcin), *Col1a1* (collagen type 1α1), and *Ccn1* (cellular communication network factor 1)]; and canonical Wnt signaling-related genes [*Lpr5* (low density lipoprotein receptor-related protein 5), *Axin2*, and *Ctnnb1* (β-catenin)] (Fig. 4a–c, gene expression was normalized to 18S rRNA). All three sets of genes were more highly expressed in females compared to males, but without differences between female *Prkg2*-WT and OB *Prkg2*-KO mice (Fig. 4a–c). *Fos*, *Alpl* (alkaline phosphatase), *Wnt10*, and *Lef1* (lymphoid enhancer binding factor-1) mRNA expression followed the same pattern, while expression of *Wnt3a* and the housekeeping genes *Hprt* (hypoxanthine phosphoribosyltransferase) and *Tuba1* (tubulin-α1) was similar in bones of male and female *Prkg2*-WT and OB *Prkg2*-KO mice (Fig. 4a–c). The male-female differences in mRNA abundance of β-catenin (C*tnnb1*) and several of its target genes (*Axin2, Lef1, Ccnd1*, and *Ccn1*) were confirmed in a separate cohort of 12 week-old wild type, non-floxed C57BL/6NHsd mice (Suppl. Fig. 4). Total β-catenin protein was reduced by ~ 50% in tibial extracts of male OB *Prkg2*-KO mice compared to male and female *Prkg2*-WT mice and female KO mice (Fig. 4d).

Expression of osteoclast-related genes was similar in both genotypes and sexes: *Acp5* (tartrate-resistant acid phosphatase), *Ctsk* (cathepsin K), *Tnfsf11* (RANKL), and *Tnfrsf11b* (osteoprotegerin) (Fig. 4e).

Primary osteoblasts from male OB Prkg2-KO mice show cell-autonomous defects in differentiation and Wnt/β-catenin-related gene expression.

We next examined the effects of PKG2 deficiency in primary osteoblasts (POBs) isolated from long bones of 12 week-old male and female *OB Prkg2-KO* mice and wild type litter mates; we generated independent cell lines from at least three mice per sex and genotype. We confirmed >80% and >90% knockdown of *Prkg2* mRNA and PKG2 protein, respectively, in osteoblasts derived from male and female OB *Prkg2*-KO mice without any change in expression of *Prkg1* mRNA (Fig. 5a,b).

A cell-permeable cGMP analog (8-CPT-cGMP) increased proliferation in osteoblasts derived from *Prkg2*-WT mice of both sexes, but it did not increase proliferation in osteoblasts from OB *Prkg2*-KO mice of either sex (Fig. 5c). Correspondingly, 8-CPT-cGMP did not activate ERK1/2 or Akt in PKG2-deficient osteoblasts of either sex, consistent with previous data that cGMP-induced activation of ERK1/2 and Akt requires PKG2 (Suppl. Fig. 5a).[5,32]

Cyclin D (*Ccnd1*) and *Fos* mRNA expression was lower in primary osteoblasts derived from male, but not female OB *Prkg2*-KO mice compared to their respective *Prkg2*-WT counterparts (Fig. 5d; *Hprt* was not altered). Osteoblasts from male and female OB *Prkg2*-KO mice showed a greater degree of apoptosis than *Prkg2*-WT cells in the presence or absence of serum (Suppl. Fig. 5b).

Osteoblasts from male OB *Prkg2*-KO mice exhibited impaired differentiation, as evident by reduced expression of osteoblast differentiation-related genes (*Bglap2 and Alpl*), decreased alkaline phosphatase activity, and diminished mineralization capacity after 14 d in differentiation medium (Fig. 5e–g). These experiments were performed in post-confluent cultures and were therefore not affected by differences in proliferation rates. The male PKG2-deficient POBs also showed reduced expression of genes related to Wnt/β-catenin signaling (*Wnt3a, Lrp5*, and *Axin2*) compared to control cells (Fig. 5h). We found no difference in differentiation capacity and Wnt-related gene expression between female osteoblasts from *Prkg2*-WT and OB *Prkg2*-KO mice (Fig. 5e–h). When comparing male and female WT osteoblasts, female cells contained a higher abundance of cyclin D1 mRNA (*Ccnd1*), osteoblast differentiation-related and Wnt/β-catenin-related transcripts (Fig. 5d, e, h).

These results in POBs are consistent with the findings in tibial bone (Fig. 4a–c), and indicate PKG2 deficiency compromises differentiation and β-catenin signaling in male, but not in female osteoblasts; however, PKG2-deficient osteoblasts from both sexes lack a proliferative response to cGMP and are more susceptible to apoptosis, compared to control cells.

Male OB Prkg2-KO mice show impaired responses to mechanical loading.

To examine whether PKG2 is involved in the response of bone to mechanical stimulation *in vivo*, we subjected adult, 20 week-old OB *Prkg2*-KO mice and their wild type litter mates to cyclic compression of the left tibia at 4 Hz, 220 cycles a day, 5 days a week for two weeks (Fig. 6a–c). The animals were anesthetized for about 15 min, and axial loading was applied through contacts at the left knee and ankle joints based on a published protocol,[42] with the contralateral tibia serving as an non-loaded control. All mice exhibited normal ambulatory activity between loading episodes, and body weights were similar in the OB *Prkg2*-KO and *Prkg2*-WT mice before and after two weeks of loading (Fig. 6d). Preliminary experiments showed that peak loads of 8 N and 7 N produced similar peak strains of ~1400 με on the anteromedial mid-diaphyseal surface of the tibia in male and female *Prkg2*-WT mice, respectively, and peak loads of 8 N produced only slightly higher strains in male OB *Prkg2*-KO mice compared to male WT littermates (Suppl. Fig. 6a). Similar results have been reported in 17 or 22 week-old C57BL/6 mice, where axial tibial loading of male mice with 8 N and female mice with 7 N also produced similar strains in both sexes.[41,49]

After two weeks of tibial loading, we analyzed cortical bone in the proximal 1/3 of the tibia, where maximal load-induced bone apposition occurred in both male and female WT mice (Suppl.Fig. 6b). Peak loads of 8 N in male and and 7 N in female mice yielded similar changes in cortical bone area and thickness in *Prkg2*-WT animals of both sexes, with ΔCt.Ar and ΔCt.Th measured as the difference between loaded and non-loaded tibia (Fig. 6e,f and Suppl. Fig. 6c; Suppl. Fig. 6d,e show the data as % change in Ct.Ar and Ct.Th, respectively, relative to the non-loaded tibia). However, the loading-induced changes in cortical bone area (ΔCt.Ar) and thickness (ΔCt.Th) in male OB *Prkg2*-KO mice were significantly less than those observed in *Prkg2*-WT litter mates, whereas female OB *Prkg2*-KO and *Prkg2*-WT mice showed similar responses to loading (Fig. 6e,f and Suppl.Fig. 6c–e). At higher loads, we observed joint damage in a majority of the mice, manifested by ankle swelling and

limping, and exuberant woven bone formation in the tibia; other workers have noted similar adverse effects.[43]

To examine loading-induced bone formation histologically, we injected mice with calcein and alizarin complexone seven and three days before euthanasia, respectively, and found robust double-labeling of periosteal surfaces of the loaded tibiae in male and female *Prkg2*-WT mice, with little periosteal labeling in the contralateral, unloaded bones (Fig. 6g and Suppl.Fig. 7a). In male OB *Prkg2*-KO mice, we observed only faint single labeling in both loaded and unloaded tibiae, wheras female OB *Prkg2*-KO mice showed load-induced periosteal labeling comparable to their *Prkg2*-WT litter mates (Fig. 6g and Suppl.Fig. 7a). Mineral apposition rates calculated from inter-label distances at the the anterior-medial aspect of the loaded tibiae (the tibial ridge, as shown in Suppl. Fig. 7b) were very similar for male and female *Prkg2*-WT and female OB *Prkg2*-KO mice (1.1 ± 0.1 μm/d; mean +/− S.D. for n=5 mice per group), but the rates were not measurable in male OB *Prkg2*-KO mice (Suppl.Fig. 7c).

To examine mechanism(s) responsible for the impaired osteogenic response to mechanical loading in the male OB *Prkg2*-KO mice, we assessed expression of several candidate genes implicated in skeletal adaptation to loading.[50–54] Three hours after a single episode of cyclical loading, cyclooxygenase-2 (*Ptgs2*), connexin-43 (*Gja1*), *Wnt10b*, the Wnt co-receptor frizzled-2 (*Fzd2*), and β-catenin (*Ctnnb1*) transcripts increased two- to three-fold in loaded tibiae compared to unloaded contralateral tibiae in both male and female *Prkg2*-WT mice (Fig. 6h). However, no increase occurred in male OB *Prkg2*-KO mice, although female OB *Prkg2*-KO mice showed normal loading responses (Fig. 6h). Loading suppressed mRNA expression of the Wnt inhibitor sclerostin (*Sost*) in *Prkg2*-WT mice of both sexes, but not in male OB *Prkg2*-KO mice (Fig. 6h; *Hprt* mRNA was not affected by loading in any of the mice). Thus, male, but not female OB *Prkg2*-KO mice showed defective mechanotransduction and failed to up-regulate cyclooxygenase-2, connexin-43, and several Wnt pathway-related genes known to contribute to the load-induced bone anabolic response.[50–53,55]

DISCUSSION

The Wnt pathway is a master regulator of skeletal homeostasis, controlling osteoblast proliferation, differentiation, and survival.[1,56] Activation of the canonical Wnt pathway culminates in cellular accumulation of β-catenin, which translocates to the nucleus and interacts with T-cell factor or lymphoid enhancer factor (LEF1) to regulate transcription of target genes, i.e., *Ccnd1*, *Axin-2*, and *Ccn1*.[1,56] Mutations in Wnt pathway components such as the Wnt co-receptor LRP-5 or the Wnt inhibitor sclerostin (*Sost*) cause severe skeletal disorders in mice and man, with increased or decreased pathway activity leading to high or low bone mass phenotypes, respectively.[56] In studies that included both sexes, *Lrp5* deficiency or osteocyte-specific *Ctnnb1* (β-catenin) haploinsufficiency reduced bone volumes more severely in male compared to female mice, while global *Sost* knockout affected females more than males.[57–59] Some of these sex differences may translate to humans, e.g., certain *LRP5* polymorphisms are associated with low bone mineral density only in men; however, *LRP5* mutations causing osteoporosis-pseudoglioma syndrome

affect both sexes.[60,61] The molecular mechanisms responsible for sexual dimorphic Wnt/β-catenin signaling are not known.

We found that male, but not female OB *Prkg2*-KO mice showed reduced bone formation and lower trabecular and cortical bone mass compared to their *Prkg2*-WT littermates. These findings are consistent with our previous studies in mice with osteoblast-specific expression of a constitutively-activate PKG2 ($PKG2^{R242Q}$): males, but not females showed increased bone formation and bone mass compared to their wild type littermates.[62] The altered bone formation and bone mass in male OB *Prkg2*-KO mice and osteoblast-specific $PKG2^{R242Q}$ transgenic mice are at least partly explained by decreased or increased Wnt/β-catenin-related gene expression in male KO or transgenic mice, respectively, compared to their wild type litter mates. In contrast, osteoblast-specific PKG2 deletion or transgenic overexpression had no effect on Wnt/β-catenin-related gene expression and no skeletal phenotype in female mice.

We have shown previously that PKG2 activation in osteoblasts leads to inhibition of glycogen synthase kinase (GSK)-3β, thereby reducing proteosomal degradation of β-catenin and stimulating its nuclear translocation.[13,32,63] POBs from male $PKG2^{R242Q}$ transgenic mice showed more nuclear β-catenin staining under basal and cGMP-stimulated conditions and β-catenin target gene expression compared to wild type POBs.[62] Correspondingly, the reduced β-catenin target gene expression in osteoblasts and bones from male OB *Prkg2*-KO mice may be partly due to lack of post-transcriptional β-catenin regulation by PKG2. Since *Lrp5* haploinsufficiency leads to low bone mass in mice,[57] the >50% decrease in *Lrp5* mRNA seen in osteoblasts and bones of male OB *Prkg2*-KO mice likely contributes to their low bone mass. Lower basal Wnt/β-catenin and *Lrp5* mRNA expression may make male mice (compared to females) more susceptible to the effects of PKG2 deficiency, and it will be important to determine whether higher levels of estrogen receptor (ER) and/or estrogens in female mice compensate for lack of PKG2 signaling in osteoblasts.

The higher expression of β-catenin mRNA and its target genes in female compared to male osteoblasts could be related to direct interactions between ER-α and β-catenin, which result in increased transcriptional activity of both proteins (β-catenin autoregulates its own promoter).[64] Consistent with this hypothesis, ER-α mutations that disrupt ER-α/β-catenin interactions suppress Wnt signaling.[65] ER-α/β-catenin cross-talk may not fully explain the sex differences in Wnt/β-catenin signalling, because the androgen receptor can also interact with β-catenin with mutual transcriptional enhancement, although the outcomes of these interactions may differ depending on the cellular background.[66,67]

Osteoprotegerin (*Tnfrsf11b*) transcription is regulated by β-catenin in calvarial osteoblasts and is reduced 30–50% in bones of osteoblast/osteocyte-specific β-catenin KO mice, resulting in increased osteoclast numbers.[68–70] However, conflicting results exist, since mice with osteoblast/osteocyte-specific *Lrp5* loss- or gain-of-function do not have altered *Tnfrsf11b* mRNA or osteoclast number/activity despite evidence of decreased or increased β-catenin signaling, respectively.[71,72] Similarly, *Tnfrsf11b* mRNA and osteoclasts were not affected in mice with osteoblast-specific *Prkg2* loss- or gain-of-function,[62] despite altered expression of β-catenin and some of its target genes. These discrepancies suggest that

β-catenin regulation of its target genes is complex, and that different genetic backgrounds of mice or β-catenin interaction with T-cell factor *versus* LEF1 in newborn *versus* adult POBs could be important in target gene expression.

We showed previously that PKG2 is required for activation of Src, ERK, and Akt in fluid shear-stressed osteoblasts, as part of a mechano-sensitive complex in osteoblast membranes.[5,32,73] PKG2 phosphorylates and activates the phosphatases Shp1 and Shp2, which in turn activate Src, Ras/Raf/MEK/ERK, and PI3K/PDK1/Akt pathways.[5,32] These data led us to hypothesize that PKG2 plays a key role in osteoblast mechanotransduction *in vivo*. In the present work, we studied mechanotransduction by subjecting mice to non-invasive tibial loading, which models natural locomotion in terms of strain distribution.[40] We chose peak loads that produced comparable strains and induced similar changes in cortical bone area and thickness in male and female *Prkg2*-WT mice; these loads produced significantly less cortical bone apposition in male OB *Prkg2*-KO mice, whereas female KO mice responded normally. Male OB *Prkg2*-KO mice experienced only slightly higher strains in response to 8 N compared to *Prkg2*-WT males, perhaps related to their lower cortical bone area, although we cannot exclude the possibility that material property changes in the bones of OB *Prkg2*-KO mice could affect load-induced strain. Other limitations of our tibial loading studies include the the lack of histomorphometric indices derived from entire tibial cross-sections. Although axial tibial loading is thought to closely mimic natural locomotion in terms of strain distribution, strains are higher than those encountered with walking or jumping, and are distributed unevenly as a result of the bones' complex geometry.[40,74]

Male OB *Prkg2*-KO mice showed an impaired transcriptional response three hours after axial loading, with decreased transcription of mechano-sensitive genes such as *Ctnnb1* (β-catenin) and *Gja1* (a β-catenin target gene); the KO mice also had low basal mRNA levels of these genes, suggesting that PKG2 acts upstream of β-catenin. Likewise, the loading-induced increase in *Ptgs2* mRNA (alias *Cox-2)* was impaired in male OB *Prkg2*-KO mice. In osteoblasts exposed to fluid sheer stress (FSS), transcriptional stimulation of *Ptgs2* requires a FSS-induced increase in intracellular calcium concentration, activation of ERK and Akt, and recruitment of AP1, C/EBP-β, and p-CREB to the *Ptgs2* promoter.[75–77] We previously showed that FSS induces *Ptgs2* mRNA via two calcium-dependent pathways involving NO/cGMP/PKG2 and FAK, respectively; both pathways converge and cooperate to activate Src, ERK, and Akt.[32] Mechanotransduction via a calcium/Akt pathway also appears to underlie suppression of *Sost* mRNA in stretched osteocytes, which mimics the transcriptional downregulation of *Sost* (Sclerostin) during ulnar loading.[54,55,78] These data suggest that PKG2 plays a key role in bone mechanotransduction in males, and suggest that females may rely more on alternative signaling pathways, such as FAK.

The sexual dimorphism we found in the loading response of bone is unusual, although many studies of skeletal adaptation to loading have included only one sex.[43,79–81] *Lrp5* deficiency or osteocyte-specific *Ctnnb1* (β-catenin) haploinsufficiency abolish the anabolic bone response to loading in both male and female mice.[41,57,82] *In vitro*, *Lrp5*-deficient osteoblasts show preserved early responses to fluid shear stress, such as ERK activation, but reduced late responses, such as osteopontin synthesis; in contrast, PKG2-deficient osteoblasts lack shear-induced ERK (and Akt) activation.[5,57]

ER-α plays an integral role in mechanotransduction. ERα-deficient osteoblasts show defective responses to mechanical strain, including impaired ERK and Akt activation, and nuclear translocation of β-catenin.[52,83,84] Cortical responses to tibial loading are lower in female but higher in male mice with global ER-α knockout.[85] However, counterintuitively, female mice with osteoblast/osteocyte-specific ER-α knockout form more bone in response to tibial loading than littermate controls, whereas loading responses in males are not affected.[43,86] Androgen receptor involvement in mechanotransduction has been examined only in male mice with global AR knockout; they also show increased load-induced periosteal bone formation compared to wild type mice, but results may be affected by altered testosterone levels.[87] It will be important to determine how ER-α and the androgen receptor regulate Wnt/β-catenin signaling in female and male osteoblasts, respectively. We have recently identified novel cross-talk between PKG2 and the androgen receptor, which may explain the sexual dimorphism in OB *Prkg2*-KO mice (manuscript submitted).

In conclusion, both PKG2 loss- and gain-of-function in osteoblasts produce striking skeletal phenotypes and establish PKG2 as a key Wnt/β-catenin regulator and mechanosensor in male mice. Therefore, FDA-approved drugs that increase cGMP, such as riociguat and tadalafil, might represent novel treatment options for osteoporosis in males, but probably also in post-menopausal females, consistent with pre-clinical data in male diabetic mice and female ovariectomized mice.[8,19,45]

Supplementary Material

Refer to Web version on PubMed Central for supplementary material.

ACKNOWLEDGMENTS:

We are grateful to Dr Ju Chen of UCSD for providing the targeting vector pDLNL, and to the staff of the UC San Diego Transgenic and Gene Targeting Core for help in generating the OB Prkg2-KO mice. We also thank Dr. Shunhui Zhuang for his expert technical assistance.

Funding:

This work was supported by the National Institutes of Health grants R01-AR-068601 and R01-AG070778 (to RBP) and P30-NS047101 (UCSD Microscopy Shared Facility).

DATA AND MATERIALS AVAILABILITY:

The data that support the findings of this study are available from the corresponding author upon request. Vectors and mice generated for this manuscript are available with via UCSD Material Transfer Agreement.

REFERENCES

1. Zaidi M, Yuen T, Sun L, Rosen CJ. Regulation of skeletal homeostasis. Endocr Rev. 2018;39(5):701–18. Epub 2018/06/14. [PubMed: 29897433]
2. Dallas SL, Prideaux M, Bonewald LF. The osteocyte: An endocrine cell … And more. Endocr Rev. 2013;34(5):658–90. [PubMed: 23612223]

3. Zaman G, Pitsillides AA, Rawlinson SC, Suswillo RF, Mosley JR, Cheng MZ, et al. Mechanical strain stimulates nitric oxide production by rapid activation of endothelial nitric oxide synthase in osteocytes. J Bone Miner Res. 1999;14(7):1123–31. [PubMed: 10404012]
4. Klein-Nulend J, Helfrich MH, Sterck JG, MacPherson H, Joldersma M, Ralston SH, et al. Nitric oxide response to shear stress by human bone cell cultures is endothelial nitric oxide synthase dependent. Biochem Biophys Res Commun. 1998;250(1):108–14. [PubMed: 9735341]
5. Rangaswami H, Schwappacher R, Marathe N, Zhuang S, Casteel DE, Haas B, et al. Cyclic Gmp and protein kinase G control a src-containing mechanosome in osteoblasts. Sci Signal. 2010;3(153):ra91.
6. Marathe N, Rangaswami H, Zhuang S, Boss GR, Pilz RB. Pro-survival effects of 17-beta-estradiol on osteocytes are mediated by nitric oxide/cGmp via differential actions of cGmp-dependent protein kinases I and II. J Biol Chem. 2012;287(2):978–88. [PubMed: 22117068]
7. Kalyanaraman H, Schwappacher R, Joshua J, Zhuang S, Scott BT, Klos M, et al. Nongenomic thyroid hormone signaling occurs through a plasma membrane-localized receptor. Sci Signal. 2014;7(326):ra48.
8. Kalyanaraman H, Schwaerzer G, Ramdani G, Castillo F, Scott BT, Dillmann W, et al. Protein kinase G activation reverses oxidative stress and restores osteoblast function and bone formation in male mice with type 1 diabetes. Diabetes. 2018;67(4):607–23. Epub 2018/01/06. [PubMed: 29301852]
9. Zheng H, Yu X, Collin-Osdoby P, Osdoby P. Rankl stimulates inducible nitric-oxide synthase expression and nitric oxide production in developing osteoclasts. An autocrine negative feedback mechanism triggered by rankl-induced interferon-beta via NF-kappaB that restrains osteoclastogenesis and bone resorption. J Biol Chem. 2006;281(23):15809–20. [PubMed: 16613848]
10. Farah C, Michel LYM, Balligand JL. Nitric oxide signalling in cardiovascular health and disease. Nat Rev Cardiol. 2018;15(5):292–316. [PubMed: 29388567]
11. Kalyanaraman H, Schall N, Pilz RB. Nitric oxide and cyclic gmp functions in bone. Nitric Oxide. 2018;76:62–70. Epub 2018/03/20. [PubMed: 29550520]
12. Yaroslavskiy BB, Li Y, Ferguson DJ, Kalla SE, Oakley JI, Blair HC. Autocrine and paracrine nitric oxide regulate attachment of human osteoclasts. J Cell Biochem. 2004;91(5):962–72. [PubMed: 15034931]
13. Kalyanaraman H, Ramdani G, Joshua J, Schall N, Boss GR, Cory E, et al. A novel, direct no donor regulates osteoblast and osteoclast functions and increases bone mass in ovariectomized mice. J Bone Miner Res. 2017;32(1):46–59. [PubMed: 27391172]
14. Hukkanen M, Platts LA, Lawes T, Girgis SI, Konttinen YT, Goodship AE, et al. Effect of nitric oxide donor nitroglycerin on bone mineral density in a rat model of estrogen deficiency-induced osteopenia. Bone. 2003;32(2):142–9. [PubMed: 12633786]
15. Turner CH, Owan I, Jacob DS, McClintock R, Peacock M. Effects of nitric oxide synthase inhibitors on bone formation in rats. Bone. 1997;21(6):487–90. [PubMed: 9430237]
16. Joshua J, Kalyanaraman H, Marathe N, Pilz RB. Nitric oxide as a mediator of estrogen effects in osteocytes. Vitam Horm. 2014;96:247–63. [PubMed: 25189390]
17. Hayashi M, Nakashima T, Yoshimura N, Okamoto K, Tanaka S, Takayanagi H. Autoregulation of osteocyte Sema3a orchestrates estrogen action and counteracts bone aging. Cell Metab. 2019;29(3):627–37 e5. Epub 2019/01/22. [PubMed: 30661929]
18. Kim SM, Taneja C, Perez-Pena H, Ryu V, Gumerova A, Li W, et al. Repurposing erectile dysfunction drugs tadalafil and vardenafil to increase bone mass. Proc Natl Acad Sci U S A. 2020;117(25):14386–94. Epub 2020/06/10. [PubMed: 32513693]
19. Pal S, Rashid M, Singh SK, Porwal K, Singh P, Mohamed R, et al. Skeletal restoration by phosphodiesterase 5 inhibitors in osteopenic mice: Evidence of osteoanabolic and osteoangiogenic effects of the drugs. Bone. 2020;135:115305. Epub 2020/03/04. [PubMed: 32126313]
20. Armour KE, Armour KJ, Gallagher ME, Godecke A, Helfrich MH, Reid DM, et al. Defective bone formation and anabolic response to exogenous estrogen in mice with targeted disruption of endothelial nitric oxide synthase. Endocrinology. 2001;142(2):760–6. [PubMed: 11159848]
21. Aguirre J, Buttery L, O'Shaughnessy M, Afzal F, de Marticorena IF, Hukkanen M, et al. Endothelial nitric oxide synthase gene-deficient mice demonstrate marked retardation in postnatal

bone formation, reduced bone volume, and defects in osteoblast maturation and activity. Am J Pathol. 2001;158:247–57. [PubMed: 11141498]

22. Grassi F, Fan X, Rahnert J, Weitzmann MN, Pacifici R, Nanes MS, et al. Bone re/modeling is more dynamic in the endothelial nitric oxide synthase(−/−) mouse. Endocrinology. 2006;147(9):4392–9. [PubMed: 16763060]
23. Rejnmark L, Vestergaard P, Mosekilde L. Decreased fracture risk in users of organic nitrates: A nationwide case-control study. J Bone Miner Res. 2006;21(11):1811–7. [PubMed: 17054422]
24. Pouwels S, Lalmohamed A, van ST, Cooper C, Souverein P, Leufkens HG, et al. Use of organic nitrates and the risk of hip fracture: A population-based case-control study. J Clin Endocrinol Metab. 2010;95(4):1924–31. [PubMed: 20130070]
25. Jamal SA, Browner WS, Bauer DC, Cummings SR. Intermittent use of nitrates increases bone mineral density: The study of osteoporotic fractures. J Bone Miner Res. 1998;13(11):1755–9. [PubMed: 9797485]
26. Jamal SA, Cummings SR, Hawker GA. Isosorbide mononitrate increases bone formation and decreases bone resorption in postmenopausal women: A randomized trial. J Bone Miner Res. 2004;19(9):1512–7. [PubMed: 15312252]
27. Wimalawansa SJ. Nitroglycerin therapy is as efficacious as standard estrogen replacement therapy (premarin) in prevention of oophorectomy-induced bone loss: A human pilot clinical study. J Bone Miner Res. 2000;15(11):2240–4. [PubMed: 11092405]
28. Nabhan AF, Rabie NH. Isosorbide mononitrate versus alendronate for postmenopausal osteoporosis. Int J Gynaecol Obstet. 2008;103(3):213–6. [PubMed: 18805524]
29. Wimalawansa SJ, Grimes JP, Wilson AC, Hoover DR. Transdermal nitroglycerin therapy may not prevent early postmenopausal bone loss. J Clin Endocrinol Metab. 2009;94(9):3356–64. [PubMed: 19549739]
30. Kapur S, Baylink DJ, Lau KH. Fluid flow shear stress stimulates human osteoblast proliferation and differentiation through multiple interacting and competing signal transduction pathways. Bone. 2003;32(3):241–51. [PubMed: 12667551]
31. Tan SD, Bakker AD, Semeins CM, Kuijpers-Jagtman AM, Klein-Nulend J. Inhibition of osteocyte apoptosis by fluid flow is mediated by nitric oxide. Biochem Biophys Res Commun. 2008;369(4):1150–4. [PubMed: 18339304]
32. Rangaswami H, Schwappacher R, Tran T, Chan GC, Zhuang S, Boss GR, et al. Protein kinase G and focal adhesion kinase converge on src/akt/beta-catenin signaling module in osteoblast mechanotransduction. J Biol Chem. 2012;287(25):21509–19. [PubMed: 22563076]
33. Watanuki M, Sakai A, Sakata T, Tsurukami H, Miwa M, Uchida Y, et al. Role of inducible nitric oxide synthase in skeletal adaptation to acute increases in mechanical loading. J Bone Miner Res. 2002;17(6):1015–25. [PubMed: 12054156]
34. Pfeifer A, Aszòdi A, Seidler U, Ruth P, Hofmann F, Fässler R. Intestinal secretory defects and dwarfism in mice lacking cGmp-dependent protein kinase II. Science. 1996;274:2082–6. [PubMed: 8953039]
35. Chikuda H, Kugimiya F, Hoshi K, Ikeda T, Ogasawara T, Shimoaka T, et al. Cyclic Gmp-dependent protein kinase II is a molecular switch from proliferation to hypertrophic differentiation of chondrocytes. Genes Dev. 2004;18(19):2418–29. [PubMed: 15466490]
36. Bonnet C, Andrieux J, Beri-Dexheimer M, Leheup B, Boute O, Manouvrier S, et al. Microdeletion at chromosome 4q21 defines a new emerging syndrome with marked growth restriction, mental retardation and absent or severely delayed speech. J Med Genet. 2010;47(6):377–84. [PubMed: 20522426]
37. Rowe DW, Adams DJ, Hong SH, Zhang C, Shin DG, Renata Rydzik C, et al. Screening gene knockout mice for variation in bone mass: Analysis by muct and histomorphometry. Curr Osteoporos Rep. 2018;16(2):77–94. Epub 2018/03/07. [PubMed: 29508144]
38. Nakanishi R, Akiyama H, Kimura H, Otsuki B, Shimizu M, Tsuboyama T, et al. Osteoblast-targeted expression of sFRP4 in mice results in low bone mass. J Bone Miner Res. 2008;23(2):271–7. Epub 2007/10/03. [PubMed: 17907918]
39. Melville KM, Robling AG, van der Meulen MC. In vivo axial loading of the mouse tibia. Methods Mol Biol. 2015;1226:99–115. Epub 2014/10/22. [PubMed: 25331046]

40. Stadelmann VA, Brun J, Bonnet N. Preclinical mouse models for assessing axial compression of long bones during exercise. Bonekey Rep. 2015;4:768. Epub 2016/01/21. [PubMed: 26788286]
41. Saxon LK, Jackson BF, Sugiyama T, Lanyon LE, Price JS. Analysis of multiple bone responses to graded strains above functional levels, and to disuse, in mice in vivo show that the human LRP5 G171V high bone mass mutation increases the osteogenic response to loading but that lack of LRP5 activity reduces it. Bone. 2011;49(2):184–93. Epub 2011/03/23. [PubMed: 21419885]
42. Yang H, Embry RE, Main RP. Effects of loading duration and short rest insertion on cancellous and cortical bone adaptation in the mouse tibia. PLoS One. 2017;12(1):e0169519. Epub 2017/01/12. [PubMed: 28076363]
43. Rooney AM, Ayobami OO, Kelly NH, Schimenti JC, Ross FP, van der Meulen MCH. Bone mass and adaptation to mechanical loading are sexually dimorphic in adult osteoblast-specific ER-alpha knockout mice. Bone. 2022;158:116349. Epub 2022/02/06. [PubMed: 35123146]
44. Bouxsein ML, Boyd SK, Christiansen BA, Guldberg RE, Jepsen KJ, Muller R. Guidelines for assessment of bone microstructure in rodents using micro-computed tomography. J Bone Miner Res. 2010;25(7):1468–86. Epub 2010/06/10. [PubMed: 20533309]
45. Joshua J, Schwaerzer GK, Kalyanaraman H, Cory E, Sah RS, Li M, et al. Soluble guanylate cyclase as a novel treatment target for osteoporosis. Endocrinology. 2014;155:4720–30. [PubMed: 25188528]
46. Porter A, Irwin R, Miller J, Horan DJ, Robling AG, McCabe LR. Quick and inexpensive paraffin-embedding method for dynamic bone formation analyses. Sci Rep. 2017;7:42505. Epub 2017/02/16. [PubMed: 28198415]
47. Dempster DW, Compston JE, Drezner MK, Glorieux FH, Kanis JA, Malluche H, et al. Standardized nomenclature, symbols, and units for bone histomorphometry: A 2012 update of the report of the asbmr histomorphometry nomenclature committee. J Bone Miner Res. 2013;28(1):2–17. [PubMed: 23197339]
48. Kalajzic I, Kalajzic Z, Kaliterna M, Gronowicz G, Clark SH, Lichtler AC, et al. Use of type I collagen green fluorescent protein transgenes to identify subpopulations of cells at different stages of the osteoblast lineage. J Bone Miner Res. 2002;17(1):15–25. [PubMed: 11771662]
49. Carriero A, Javaheri B, Bassir Kazeruni N, Pitsillides AA, Shefelbine SJ. Age and sex differences in load-induced tibial cortical bone surface strain maps. JBMR Plus. 2021;5(3):e10467. Epub 2021/03/30. [PubMed: 33778328]
50. Kelly NH, Schimenti JC, Ross FP, van der Meulen MC. Transcriptional profiling of cortical versus cancellous bone from mechanically-loaded murine tibiae reveals differential gene expression. Bone. 2016;86:22–9. Epub 2016/02/16. [PubMed: 26876048]
51. Lau KH, Baylink DJ, Zhou XD, Rodriguez D, Bonewald LF, Li Z, et al. Osteocyte-derived insulin-like growth factor I is essential for determining bone mechanosensitivity. Am J Physiol Endocrinol Metab. 2013;305(2):E271–81. Epub 2013/05/30. [PubMed: 23715728]
52. Armstrong VJ, Muzylak M, Sunters A, Zaman G, Saxon LK, Price JS, et al. Wnt/b-catenin signaling is a component of osteoblastic bone cell early responses to load-bearing and requires estrogen receptor a. J Biol Chem. 2007;282(28):20715–27. [PubMed: 17491024]
53. Choi RB, Robling AG. The Wnt pathway: An important control mechanism in bone's response to mechanical loading. Bone. 2021;153:116087. Epub 2021/07/17. [PubMed: 34271473]
54. Robling AG, Niziolek PJ, Baldridge LA, Condon KW, Allen MR, Alam I, et al. Mechanical stimulation of bone in vivo reduces osteocyte expression of Sost/Sclerostin. J Biol Chem. 2008;283(9):5866–75. Epub 2007/12/20. [PubMed: 18089564]
55. Tu X, Rhee Y, Condon KW, Bivi N, Allen MR, Dwyer D, et al. Sost downregulation and local wnt signaling are required for the osteogenic response to mechanical loading. Bone. 2012;50(1):209–17. Epub 2011/11/15. [PubMed: 22075208]
56. Baron R, Kneissel M. Wnt signaling in bone homeostasis and disease: From human mutations to treatments. Nat Med. 2013;19(2):179–92. [PubMed: 23389618]
57. Sawakami K, Robling AG, Ai M, Pitner ND, Liu D, Warden SJ, et al. The Wnt co-receptor LRP5 is essential for skeletal mechanotransduction but not for the anabolic bone response to parathyroid hormone treatment. J Biol Chem. 2006;281(33):23698–711. [PubMed: 16790443]

58. Maurel DB, Duan P, Farr J, Cheng AL, Johnson ML, Bonewald LF. Beta-catenin haplo insufficient male mice do not lose bone in response to hindlimb unloading. PLoS One. 2016;11(7):e0158381. [PubMed: 27410430]
59. Li X, Ominsky MS, Niu QT, Sun N, Daugherty B, D'Agostin D, et al. Targeted deletion of the sclerostin gene in mice results in increased bone formation and bone strength. J Bone Miner Res. 2008;23(6):860–9. Epub 2008/02/14. [PubMed: 18269310]
60. Ferrari SL, Deutsch S, Choudhury U, Chevalley T, Bonjour JP, Dermitzakis ET, et al. Polymorphisms in the low-density lipoprotein receptor-related protein 5 (LRP5) gene are associated with variation in vertebral bone mass, vertebral bone size, and stature in whites. Am J Hum Genet. 2004;74(5):866–75. Epub 2004/04/13. [PubMed: 15077203]
61. Gong Y, Slee RB, Fukai N, Rawadi G, Roman-Roman S, Reginato AM, et al. LDL receptor-related protein 5 (Lrp5) affects bone accrual and eye development. Cell. 2001;107(4):513–23. Epub 2001/11/24. [PubMed: 11719191]
62. Ramdani G, Schall N, Kalyanaraman H, Wahwah N, Moheize S, Lee JJ, et al. cGmp-dependent protein kinase-2 regulates bone mass and prevents diabetic bone loss. J Endocrinol. 2018;238(3):203–19. Epub 2018/06/20. [PubMed: 29914933]
63. Zhao X, Zhuang S, Chen Y, Boss GR, Pilz RB. Cyclic Gmp-dependent protein kinase regulates CCAAT enhancer-binding protein-beta functions through inhibition of glycogen synthase kinase-3. J Biol Chem. 2005;280:32683–92. [PubMed: 16055922]
64. Kouzmenko AP, Takeyama K, Ito S, Furutani T, Sawatsubashi S, Maki A, et al. Wnt/beta-catenin and estrogen signaling converge in vivo. J Biol Chem. 2004;279(39):40255–8. [PubMed: 15304487]
65. Modder UI, Rudnik V, Liu G, Khosla S, Monroe DG. A DNA binding mutation in estrogen receptor-alpha leads to suppression of Wnt signaling via beta-catenin destabilization in osteoblasts. J Cell Biochem. 2012;113(7):2248–55. [PubMed: 22573547]
66. Mulholland DJ, Dedhar S, Coetzee GA, Nelson CC. Interaction of nuclear receptors with the Wnt/beta-catenin/TCF signaling axis: Wnt you like to know? Endocr Rev. 2005;26(7):898–915. [PubMed: 16126938]
67. Schweizer L, Rizzo CA, Spires TE, Platero JS, Wu Q, Lin TA, et al. The androgen receptor can signal through Wnt/beta-catenin in prostate cancer cells as an adaptation mechanism to castration levels of androgens. BMC Cell Biol. 2008;9:4. [PubMed: 18218096]
68. Glass DA, Bialek P, Ahn JD, Starbuck M, Patel MS, Clevers H, et al. Canonical Wnt signaling in differentiated osteoblasts controls osteoclast differentiation. Dev Cell. 2005;8(5):751–64. [PubMed: 15866165]
69. Kramer I, Halleux C, Keller H, Pegurri M, Gooi JH, Weber PB, et al. Osteocyte Wnt/beta-catenin signaling is required for normal bone homeostasis. Mol Cell Biol. 2010;30(12):3071–85. [PubMed: 20404086]
70. Holmen SL, Zylstra CR, Mukherjee A, Sigler RE, Faugere MC, Bouxsein ML, et al. Essential role of beta-catenin in postnatal bone acquisition. J Biol Chem. 2005;280(22):21162–8. [PubMed: 15802266]
71. Riddle RC, Diegel CR, Leslie JM, Van Koevering KK, Faugere MC, Clemens TL, et al. Lrp5 and Lrp6 exert overlapping functions in osteoblasts during postnatal bone acquisition. PLoS One. 2013;8(5):e63323. Epub 2013/05/16. [PubMed: 23675479]
72. Cui Y, Niziolek PJ, MacDonald BT, Zylstra CR, Alenina N, Robinson DR, et al. Lrp5 functions in bone to regulate bone mass. Nat Med. 2011;17(6):684–91. Epub 2011/05/24. [PubMed: 21602802]
73. Rangaswami H, Marathe N, Zhuang S, Chen Y, Yeh JC, Frangos JA, et al. Type II cGmp-dependent protein kinase mediates osteoblast mechanotransduction. J Biol Chem. 2009; 284:14796–808. [PubMed: 19282289]
74. De Souza RL, Matsuura M, Eckstein F, Rawlinson SC, Lanyon LE, Pitsillides AA. Non-invasive axial loading of mouse tibiae increases cortical bone formation and modifies trabecular organization: A new model to study cortical and cancellous compartments in a single loaded element. Bone. 2005;37(6):810–8. Epub 2005/10/04. [PubMed: 16198164]

75. Chen NX, Ryder KD, Pavalko FM, Turner CH, Burr DB, Qiu J, et al. Ca^{2+} regulates fluid shear-induced cytoskeletal reorganization and gene expression in osteoblasts. Am J Physiol Cell Physiol. 2000;278:C989–C97. [PubMed: 10794673]
76. Ogasawara A, Arakawa T, Kaneda T, Takuma T, Sato T, Kaneko H, et al. Fluid shear stress-induced cyclooxygenase-2 expression is mediated by C/EBP-β, cAmp-response element-binding protein, and AP-1 in osteoblastic MC3T3-e1 cells. J Biol Chem. 2001;276(10):7048–54. [PubMed: 11092885]
77. Wadhwa S, Godwin SL, Peterson DR, Epstein MA, Raisz LG, Pilbeam CC. Fluid flow induction of cyclo-oxygenase 2 gene expression in osteoblasts is dependent on an extracellular signal-regulated kinase signaling pathway. J Bone Miner Res. 2002;17(2):266–74. Epub 2002/01/29. [PubMed: 11811557]
78. Sasaki F, Hayashi M, Mouri Y, Nakamura S, Adachi T, Nakashima T. Mechanotransduction via the Piezo1-Akt pathway underlies sost suppression in osteocytes. Biochem Biophys Res Commun. 2020;521(3):806–13. Epub 2019/11/12. [PubMed: 31708103]
79. Wang L, You X, Zhang L, Zhang C, Zou W. Mechanical regulation of bone remodeling. Bone Res. 2022;10(1):16. Epub 2022/02/20. [PubMed: 35181672]
80. Riddle RC, Leslie JM, Gross TS, Clemens TL. Hypoxia-inducible factor-1alpha protein negatively regulates load-induced bone formation. J Biol Chem. 2011;286(52):44449–56. Epub 2011/11/15. [PubMed: 22081627]
81. Mohan S, Bhat CG, Wergedal JE, Kesavan C. In vivo evidence of IGF-I-estrogen crosstalk in mediating the cortical bone response to mechanical strain. Bone Res. 2014;2:14007. Epub 2014/01/01. [PubMed: 26273520]
82. Kang KS, Hong JM, Robling AG. Postnatal beta-catenin deletion from DMP1-expressing osteocytes/osteoblasts reduces structural adaptation to loading, but not periosteal load-induced bone formation. Bone. 2016;88:138–45. [PubMed: 27143110]
83. Sunters A, Armstrong VJ, Zaman G, Kypta RM, Kawano Y, Lanyon LE, et al. Mechano-transduction in osteoblastic cells involves strain-regulated estrogen receptor alpha-mediated control of insulin-like growth factor (IGF) I receptor sensitivity to ambient IGF, leading to phosphatidylinositol 3-kinase/akt-dependent Wnt/Lrp5 receptor-independent activation of beta-catenin signaling. J Biol Chem. 2010;285(12):8743–58. [PubMed: 20042609]
84. Aguirre JI, Plotkin LI, Gortazar AR, Millan MM, O'Brien CA, Manolagas SC, et al. A novel ligand-independent function of the estrogen receptor is essential for osteocyte and osteoblast mechanotransduction. J Biol Chem. 2007;282(35):25501–8. [PubMed: 17609204]
85. Saxon LK, Galea G, Meakin L, Price J, Lanyon LE. Estrogen receptors alpha and beta have different gender-dependent effects on the adaptive responses to load bearing in cancellous and cortical bone. Endocrinology. 2012;153(5):2254–66. [PubMed: 22416084]
86. Melville KM, Kelly NH, Surita G, Buchalter DB, Schimenti JC, Main RP, et al. Effects of deletion of eralpha in osteoblast-lineage cells on bone mass and adaptation to mechanical loading differ in female and male mice. J Bone Miner Res. 2015;30(8):1468–80. Epub 2015/02/25. [PubMed: 25707500]
87. Callewaert F, Bakker A, Schrooten J, Van Meerbeek B, Verhoeven G, Boonen S, et al. Androgen receptor disruption increases the osteogenic response to mechanical loading in male mice. J Bone Miner Res. 2010;25(1):124–31. [PubMed: 19821763]

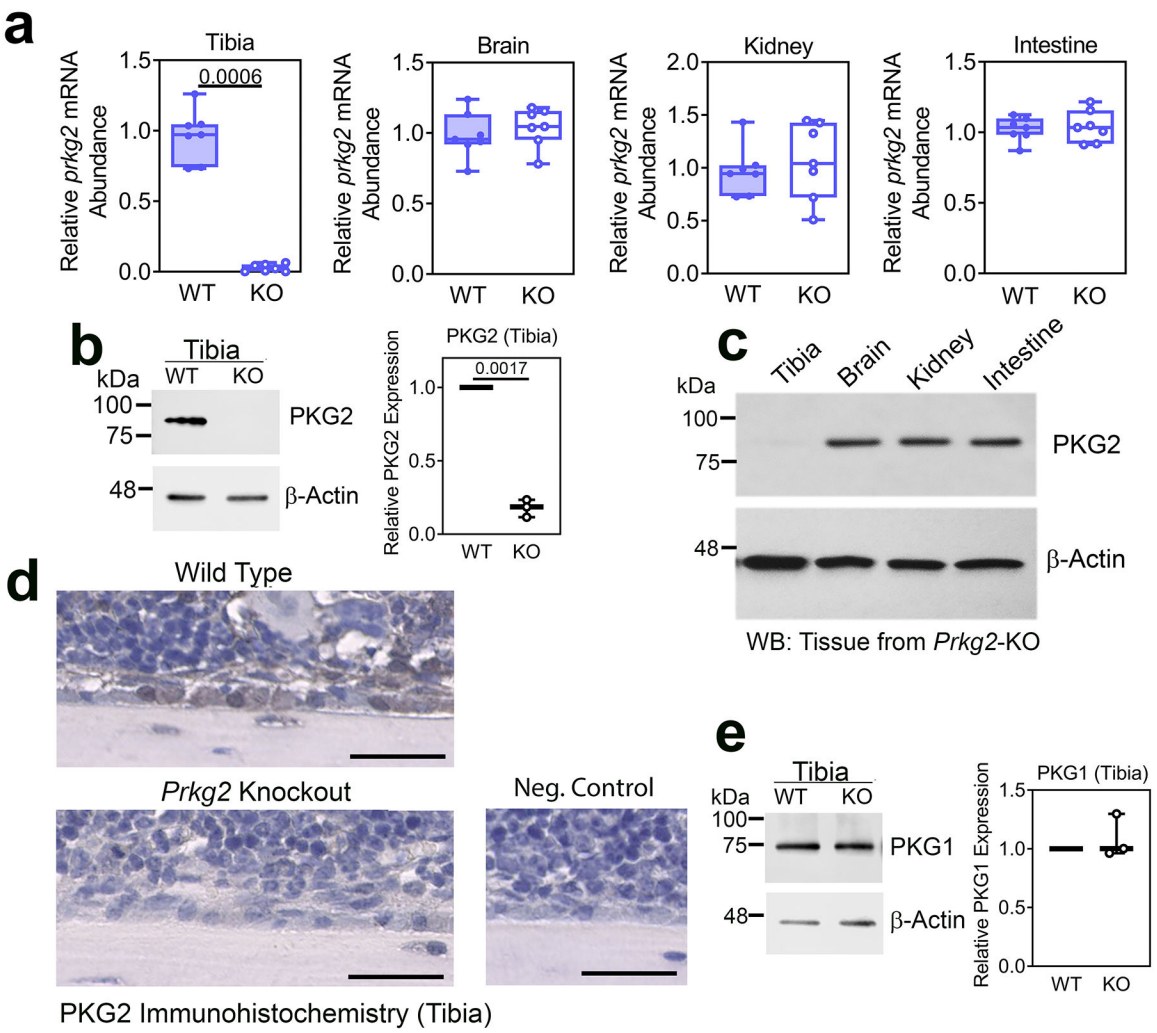

Fig. 1: Characterization of OB *Prkg2*-KO mice.

(a) *Prkg2* mRNA was measured in organs of eight week-old male mice with osteoblast-specific *Prkg2* knockout ("KO"; genotype: *Col1a1-Cre; Prkg2f/f*) and their *Prkg2*-WT litter mates ("WT"; genotype *Prkg2f/f*). Relative mRNA abundance was quantified by qRT-PCR and normalized to 18S ribosomal RNA using the ΔΔCt method, with the mean ΔCt value obtained in control animals assigned a value of one (n=7 male mice per genotype). (b) PKG2 protein was assessed by Western blotting in extracts of tibial shafts, with densitometry scanning of longer exposures of blots from n=3 male mice per genotype. (c) PKG2 protein was assessed in different tissue extracts from a male KO mouse, with β-actin serving as a loading control. (d) Immunohistochemical staining for PKG2 expression (brown) on tibial bone sections from male WT and KO mice (bar = 50 μm; negative control lacks primary antibody). (e) Type 1 PKG (PKG1) protein was assessed in the tibial extracts described in panel b. Comparisons by two-tailed Student t-test. Results for female mice are shown in Suppl. Fig. 1d–g.

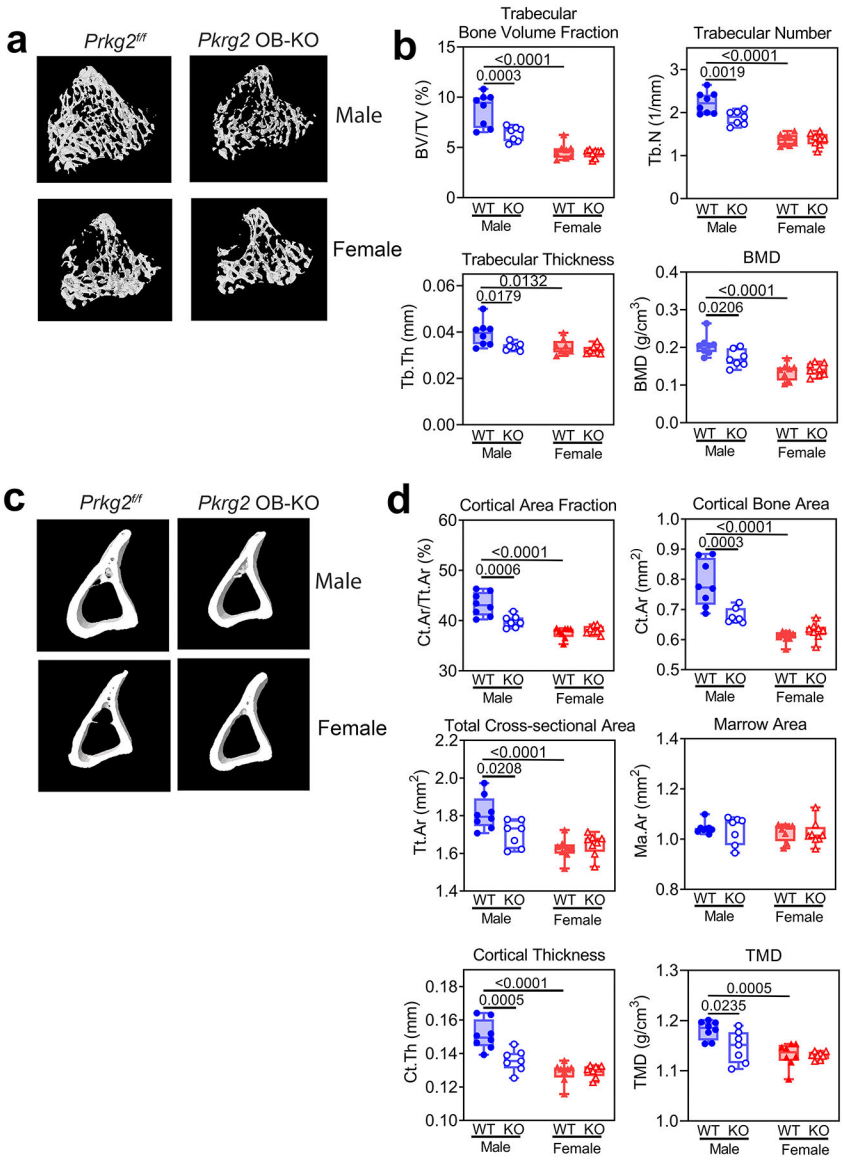

Fig. 2: Reduced bone volumes in male, but not female OB *Prkg2*-KO mice.

Osteoblast-specific *Prkg2* knockout mice (KO) and *Prkg2*-WT litter mates (WT) were euthanized at the age of eight weeks (male mice n = 8 WT and n = 7 KO; female mice n = 8 WT and n = 8 KO). (a) 3-D reconstructions of micro-CT images of trabecular bone in the proximal tibia. (b) Trabecular bone volume fraction (BV/TV), trabecular number (Tb.N), trabecular thickness (Tb.Th), and bone mineral density (BMD) were measured in the proximal tibia by micro-CT as described in Methods. (c) 3-D reconstructions of micro-CT images of cortical bone in the mid-tibia. (d) Cortical area fraction (Ct.Ar/Tt.Ar), cortical bone area (Ct.Ar), total cross-sectional area (Tt.Ar), marrow area (Ma.Ar), cortical thickness (Ct.Th), and tissue mineral density (TMD) were measured in the mid-tibial diaphysis. Comparisons by two-way ANOVA; F-values are compiled in Suppl. Table 3.

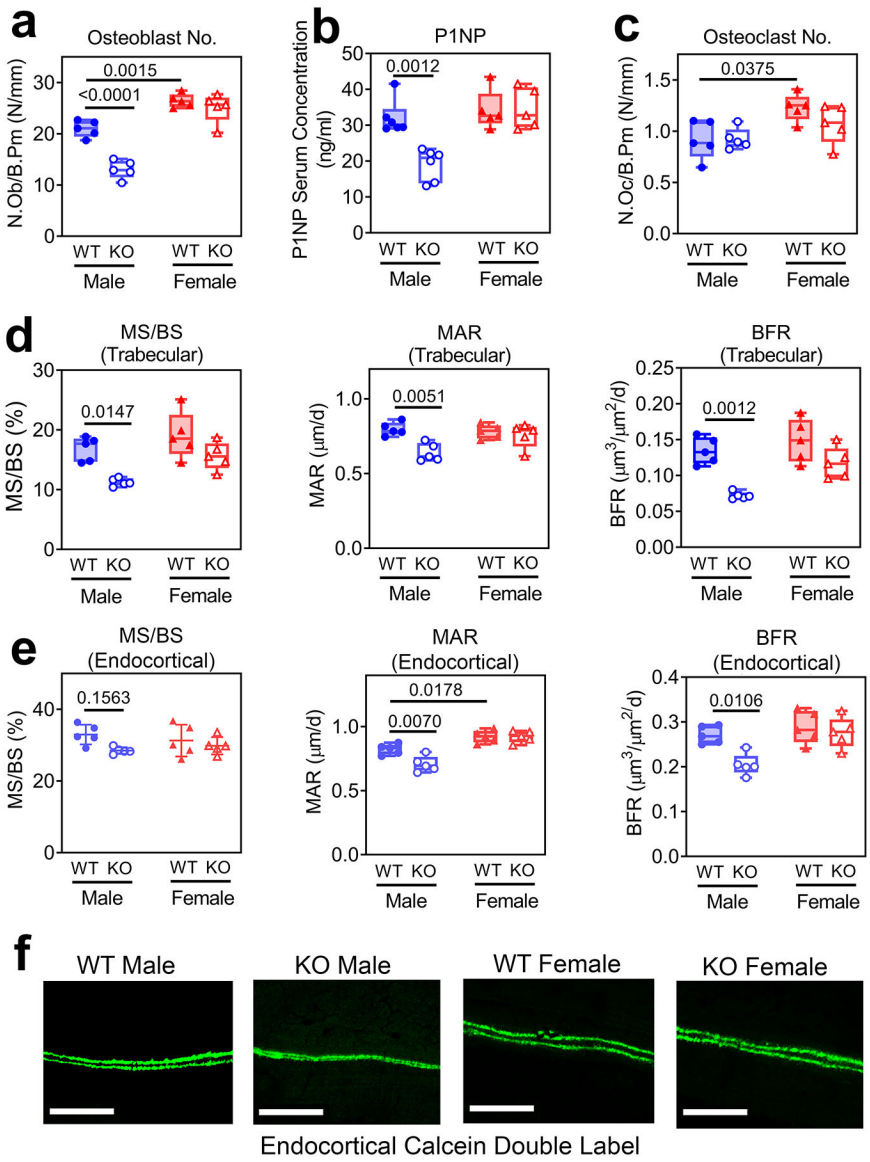

Fig. 3: Reduced osteoblast numbers and bone formation parameters in male, but not female OB *Prkg2*-KO mice.

Male and female osteoblast-specific *Prkg2* knockout mice (KO) and their *Prkg2*-WT litter mates (WT) were injected with calcein 7 and 2 d prior to euthanasia at eight weeks of age (n = 5 mice per sex and per genotype). (a) Osteoblasts were counted on trabecular surfaces of trichrome-stained sections of the distal femur (the region of interest is shown in Suppl. Fig. 3a). (b) Procollagen-1 N-terminal peptide (P1NP) was measured in serum. (c) Osteoclasts were counted on trabecular surfaces. (d) Mineralizing surfaces (MS/BS), mineral apposition rate (MAR), and bone formation rate (BFR) were measured on calcein-labelled trabecular bone surfaces of the femur. (e) The same dynamic histomorphometry parameters were measured on endocortical bone surfaces of the femur. (f) Calcein double label is shown on endocortical surfaces (bar = 25 μm). Comparisons by two-way ANOVA; F-values are in Suppl. Table 3.

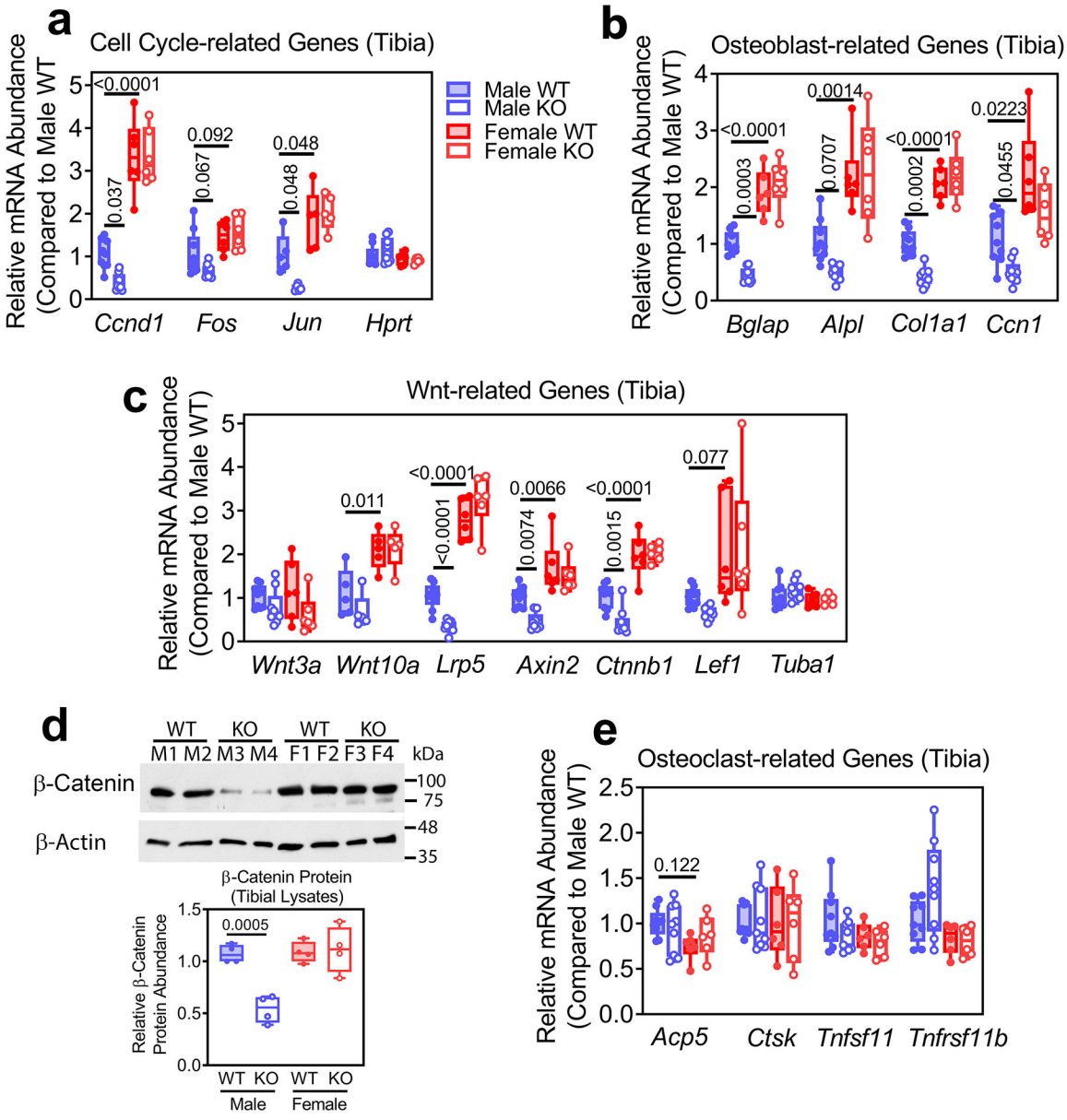

Fig. 4: Reduced expression of cell cycle-, osteoblast differentiation-, and Wnt pathway-related genes in tibiae of male, but not female OB *Prkg2*-KO mice.

Gene expression was measured in the tibial shafts of male (blue box plots) and female (red box plots) osteoblast-specific *Prkg2* knockout (KO) mice and their *Prkg2*-WT litter mates (WT) at the age of eight weeks. Relative mRNA abundance was quantified by qRT-PCR and normalized to 18S ribosomal RNA using the ΔΔCt method, with the mean ΔCt value obtained in male *Prkg2*-WT animals assigned a value of one (n = 9 male and n = 6 female mice per genotype, in panels a-c and e). (a) Cell cycle-related genes: *Ccnd1*, cyclin D1; *Fos*, c-Fos; and *Jun*, c-Jun, with *Hprt*, hypoxanthine phosphoribosyltransferase, serving as a housekeeping gene. (b) Osteoblast differentiation-related genes*: Bglap*, osteocalcin; *Alpl*, alkaline phosphatase; *Col1a1*, collagen type 1α1; and *Ccn1*, cellular communication network factor 1 (alias Cyr16, an extracellular matrix protein with signaling function). (c)

Wnt pathway-related genes: *Wnt3a; Wnt10; Lrp5*, low density lipoprotein receptor-related protein 5; *Axin2*; *Ctnnb1*, β-catenin; and *Lef1*, lymphoid enhancer binding factor-1, with *Tuba1*, tubulin-α1, serving as a housekeeping gene. (d) Total β-catenin protein assessed on Western blots of tibial shaft lysates from male (M1–4) and female (F1–4) *Prkg2*-WT (WT) and *Prkg2*-KO (KO) litter mates; β-actin served as a loading control. Quantification of blots by densitometry scanning from n=4 animals per sex and genotype is shown in the graph below. (e) Osteoclast-related genes: *Acp5*, tartrate-resistant acid phosphatase; *Ctsk*, cathepsin K; *Tnfsf11*, RANKL; and *Tnfrsf11b*, osteoprotegerin. Comparisons by two-way ANOVA; F-values are in Suppl. Table 3.

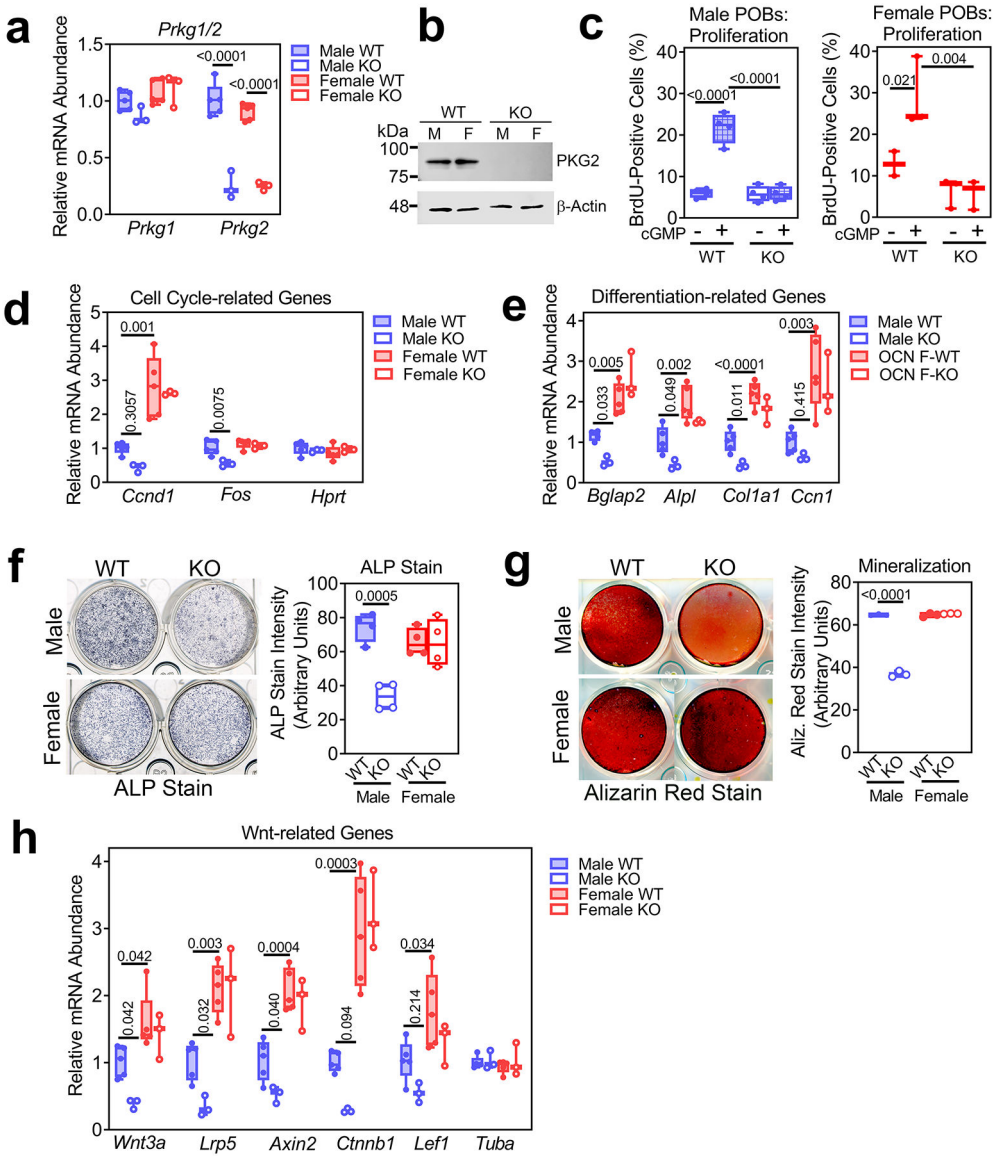

Fig.5: Phenotypic differences between male and female PKG2-deficient POBs.

Primary osteoblasts (POBs) were isolated from 12 week-old male (blue box plots) and female (red box plots) osteoblast-specific *Prkg2* knockout (KO) mice and their *Prkg2*-WT litter mates (WT). Cells were independently derived from three to four mice per sex and genotype and were matched for passage number and cell density. (a) *Prkg1* and *Prkg2* mRNA was quantified by qRT-PCR and normalized to 18S rRNA as described in Fig.1a, with the mean ΔCT values obtained in male WT cells assigned a value of one. (b) PKG2 protein was analyzed in whole cell lysates by Western blotting, with β-actin serving as a loading control. (c) WT and KO POBs were incubated for 24 h in the absence or presence of 100 μM 8-CPT-cGMP (cGMP) in medium containing 0.1% FBS and 5-bromo-2-deoxyuridine (BrdU); BrdU uptake into S-phase nuclei was determined by immunofluorescence staining. (d) Expression of *Ccnd1*, *Fos*, and *Hprt* mRNA was measured by qRT-PCR as in panel a. (e) WT and KO POBs were grown to confluency and then

transferred to differentiation medium containing ascorbate and β-glycerolphosphate for 14 d. *Bglap2*, *Alpl*, *Col1a1, Ccn1*, and *Hprt* mRNA were measured by qRT-PCR as in panel a. (f,g) Cells were stained for alkaline phosphatase activity (f) or assessed for mineralization by Alizarin Red staining (g) after 14 d in differentiation medium; staining intensity was quantified by ImageJ. (h) Cells were cultured as in panel e, and expression of Wnt pathway-related genes was measured as in panel a (gene names as in Fig. 4c), with *Tuba1* and *Hprt* serving as housekeeping genes. Comparisons by two-way ANOVA; F-values are in Suppl. Table 3.

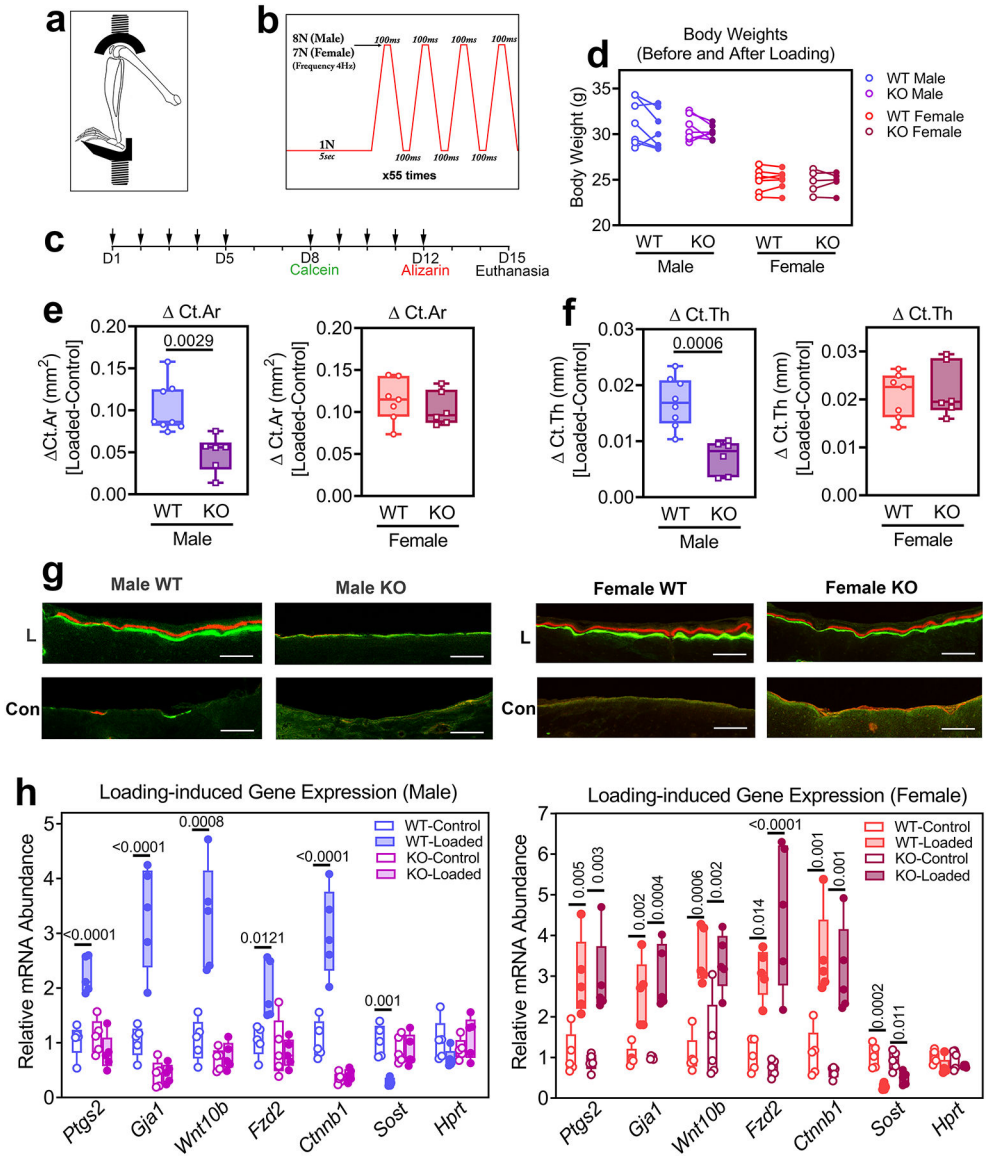

Fig. 6: Impaired response to axial tibial loading in male, but not female *OB Prkg2-KO* mice.

(a-c) 20 week-old OB *Prkg2*-KO mice and their *Prkg2*-WT litter mates (WT) were anesthetized and subjected to axial loading of the left tibia through contacts at the knee and ankle joints (a) as described in Methods, with the right tibia serving as an unloaded control. Peak loads of 8 N and 7 N were applied to male and female mice, respectively, at 4 Hz, 220 cycles a day, 5 days a week for two weeks (b). Calcein and alizarin complexone were injected 7 and 3 d prior to euthanasia to label newly-formed bone (c). (d) OB *Prkg2*-KO mice and *Prkg2*-WT littermates were weighed on days 1 and 15 of the loading experiment. (e,f) Cortical bone in the proximal third of the tibiae was assessed by mCT, and the loading-induced change in cortical bone area (ΔCt.Ar in e) and cortical thickness (ΔCt.Th in f) was calculated as the difference between loaded and unloaded tibia of each animal. Data for n = 8 male and n = 7 female WT; n = 6 male and n=6 female OB *Prkg2*-KO mice. (g) Transverse sections of methylmethacrylate-embedded tibiae were obtained 5 mm below the

tibial plateau and photographed at 20 x using a Leica SP8 Lightning confocal microscope (the bar represents 100 μm). Periosteal labeling is shown at the anterior-medial aspect of the tibia (the tibial ridge, as indicated by arrows in Suppl. Fig. 6f). (h) Three hours after a single loading episode of 220 cycles as described in panel b, mice were euthanized, and RNA extracted from loaded and unloaded tibial shafts was analyzed by RTqPCR using primers for six mechanosensitive genes: *Ptgs2*, cyclooxygenase-2; *Gja1*, connexin-43 (a β-catenin target gene); *Wnt10b*; *Fzd2*, frizzled-2 (Wnt co-receptor); *Ctnnb1*, β-catenin; and *Sost*, sclerostin (Wnt antagonist); *Hprt* served as an RNA quality control. Relative mRNA abundance was normalized to 18S ribosomal RNA, with the mean ΔCt values obtained in control (unloaded) WT tibiae assigned a value of one (n = 5 mice per sex and genotype). Comparisons by two-sided t-test (panels d, e, f), or two-way ANOVA (panel h; F-values are in Suppl. Table 3).